Cell Reports

Epidermal turnover in the planarian *Schmidtea mediterranea* involves basal cell extrusion and intestinal digestion

Graphical abstract

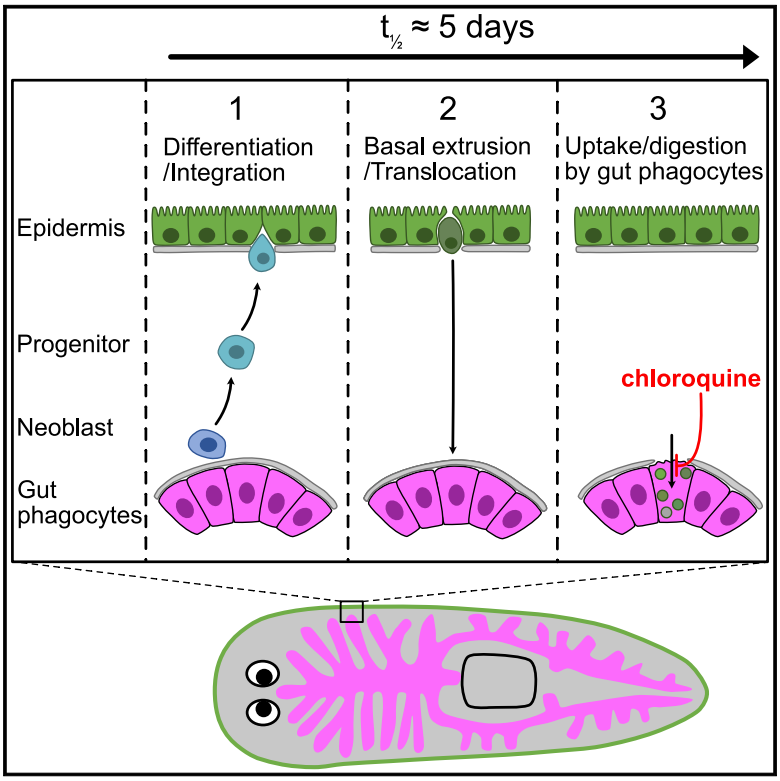

Highlights

- Planarian epidermal turnover rates differ between dorsal and ventral
- The ventral epidermis is a highly dynamic tissue with a half-life of 4.5 days
- Epidermal cells are eliminated via basal extrusion, not outward shedding
- Internalized epidermal cells are taken up and digested by gut phagocytes

Authors

Jun-Ru Lee, Tobias Boothe, Clemens Mauksch, Albert Thommen, Jochen C. Rink

Correspondence

jochen.rink@mpinat.mpg.de

In brief

Although planarians are known to continuously renew all cell types, how they remove old cells is poorly understood. By developing imaging assays to quantify and observe cell turnover in the epidermis, the authors find that epidermal cells undergo basal extrusion and that the internalized cells are digested by intestinal phagocytes.

Lee et al., 2024, Cell Reports ■■, 114305
■■, 2024
https://doi.org/10.1016/j.celrep.2024.114305

CellPress

Please cite this article in press as: Lee et al., Epidermal turnover in the planarian *Schmidtea mediterranea* involves basal cell extrusion and intestinal digestion, Cell Reports (2024), https://doi.org/10.1016/j.celrep.2024.114305

Cell Reports

CellPress
OPEN ACCESS

Report

Epidermal turnover in the planarian *Schmidtea mediterranea* involves basal cell extrusion and intestinal digestion

Jun-Ru Lee,[1,3] Tobias Boothe,[1] Clemens Mauksch,[1] Albert Thommen,[4] and Jochen C. Rink[1,2,5,*]
[1]Department of Tissue Dynamics and Regeneration, Max Planck Institute for Multidisciplinary Sciences, Am Fassberg 11, 37077 Göttingen, Germany
[2]Faculty of Biology and Psychology, Georg-August-University, Göttingen, Germany
[3]Graduate Center for Neurosciences, Biophysics, and Molecular Biosciences, University of Göttingen, 37077 Göttingen, Germany
[4]Cancer Metabolism Laboratory, The Francis Crick Institute, 1 Midland Road, London NW1 1AT, UK
[5]Lead contact
*Correspondence: jochen.rink@mpinat.mpg.de
https://doi.org/10.1016/j.celrep.2024.114305

SUMMARY

Planarian flatworms undergo continuous internal turnover, wherein old cells are replaced by the division progeny of adult pluripotent stem cells (neoblasts). How cell turnover is carried out at the organismal level remains an intriguing question in planarians and other systems. While previous studies have predominantly focused on neoblast proliferation, little is known about the processes that mediate cell loss during tissue homeostasis. Here, we use the planarian epidermis as a model to study the mechanisms of cell removal. We established a covalent dye-labeling assay and image analysis pipeline to quantify the cell turnover rate in the planarian epidermis. Our findings indicate that the ventral epidermis is highly dynamic and epidermal cells undergo internalization via basal extrusion, followed by a relocation toward the intestine and ultimately digestion by intestinal phagocytes. Overall, our study reveals a complex homeostatic process of cell clearance that may generally allow planarians to catabolize their own cells.

INTRODUCTION

Many tissues and organs exist in a state of dynamic turnover, whereby old cells are continuously replaced by the progeny of stem cells. For example, in the vertebrate intestinal epithelium, stem cells residing in the crypt continuously generate transit-amplifying cells that differentiate into epithelial cells, which gradually become displaced along the villus and delaminate once they reach the tip.[1–3] The homeostasis of the intestinal epithelium is highly dynamic, with an average lifetime of epithelial cells on the order of ~5 days.[4] Besides the precise balancing of cell divisions with cell loss exemplified by the intestinal epithelium, a further challenge in dynamic tissues is often the process of clearing the cells to be replaced. In the case of liver homeostasis, the resident sinusoidal cells phagocytose apoptotic hepatocytes.[5,6] Similarly, the zebrafish embryonic ectoderm is capable of phagocytosing dead cells.[7] In other contexts, motile and often non-tissue-resident phagocytes mediate cell clearance processes.[8] The severe pathological consequences that can result from cell clearance defects underscore the collective importance of the underlying mechanisms.[9–11]

Planarian flatworms provide a fascinating example of dynamic turnover at an organismal scale. Pluripotent adult stem cells, so-called neoblasts, are the only division-competent planarian cell type outside of the reproductive system.[12–15] They are highly abundant at >10% of all cells[16,17] and reside in the mesenchyme surrounding all internal organs. This implies that all tissue and organ progenitors are generated out of place and thus need to migrate to their target tissues during their differentiation.[18–20] Transplantation of a single pluripotent donor neoblast can rescue the demise of an irradiated host due to the re-colonialization of host tissues by descendants of the donor stem cell over the course of several months,[21] indicating that all tissues are replaced continuously by newly generated neoblast progeny. Finally, planarians do not have a fixed body size. They grow when fed and shrink during starvation, dynamically scaling the total number of organismal cells.[22,23] Overall, the combination of a single source of new cells, organismal cell turnover, and body size scaling makes planarians an intriguing model for investigating the underlying principles.

Although the dynamic nature of planarian tissue architecture has long been recognized, the field has largely focused on the generation and maturation of neoblast progenitors. The epidermal cell lineage is derived from neoblasts expressing the zinc-finger transcription factor zfp-1, whose post-mitotic progenitors undergo several differentiation stages during their outward migration and final maturation upon integration into the epidermis.[18,24–27] In addition, the rates of neoblast proliferation, and therefore likely progenitor production, vary in response to feeding or wounding.[28,29] Conversely, much less is known about

Please cite this article in press as: Lee et al., Epidermal turnover in the planarian *Schmidtea mediterranea* involves basal cell extrusion and intestinal digestion, Cell Reports (2024), https://doi.org/10.1016/j.celrep.2024.114305

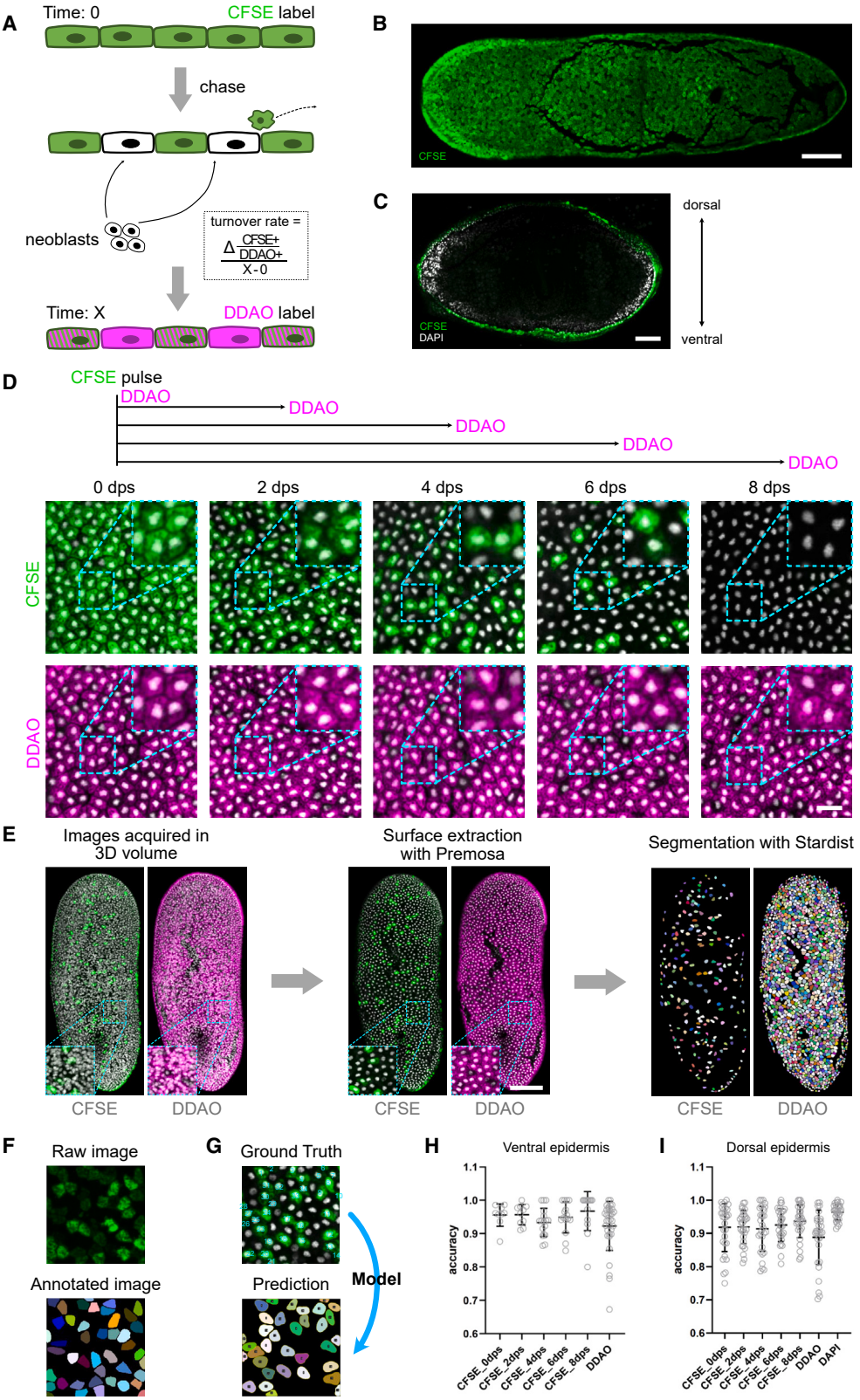

(legend on next page)

Please cite this article in press as: Lee et al., Epidermal turnover in the planarian *Schmidtea mediterranea* involves basal cell extrusion and intestinal digestion, Cell Reports (2024), https://doi.org/10.1016/j.celrep.2024.114305

the mechanisms that control cell removal during turnover. Apoptotic cell death is known to be regulated in a tissue-specific manner,[30] and cell death processes have been proposed to contribute to degrowth.[31] However, neither the mechanisms that induce cell removal nor the processes that mediate cell clearance during turnover are currently known.

In this study, we used the epidermis as a model tissue to explore cell turnover in planarians. By developing a pulse-chase labeling assay to quantify the turnover rate, we found that the half-life of epidermal cells varies greatly between the dorsal and ventral sides. We also established a live-imaging protocol to visualize the process of epidermal cell removal. Interestingly, we found that epidermal cells were internalized rather than shed to the outside. Furthermore, using dual-color live imaging and pharmacological treatments, we provide evidence that internalized epidermal cells enter the intestine and are digested by intestinal phagocytes. Taken together, we propose that the observed self-catabolism of epidermal cells by intestinal phagocytes may constitute a general principle of planarian tissue turnover.

RESULTS

Although the planarian epidermis is known to incorporate new cells on a timescale of days,[25,27,32,33] the rate of epidermal cell turnover has not been accurately measured so far. To quantify epidermal turnover, we took advantage of the selective accessibility of the epidermis to exogenously supplied substances. As cartooned in Figure 1A, we developed an assay that relies on the covalent pulse labeling of epidermal cells with a cell-permeant form of the dye carboxyfluorescein succinimidyl ester (CFSE), followed by the application of a second spectrally distinct covalent label, 7-hydroxy-9H-(1,3-dichloro-9,9-dimethylacridin-2-one) succinimidyl ester (DDAO) after a specific chase interval. Accordingly, changes in the fraction of $CFSE^+/DDAO^+$ cells during the chase period should reflect the fraction of epidermal cells that have been replaced during the chase interval. As shown in Figure 1B, CFSE pulse labeling and immediate fixation results in uniform labeling of the epidermis under our experimental conditions. The labeling pattern in cross-sections (Figure 1C) indicates labeling specificity for the epidermis. Similar results were observed for DDAO labeling (data not shown). Thus, CFSE and DDAO selectively label epidermal cells without any signal interference from the deeper tissue layers. As expected, the fraction of $CFSE^+/DDAO^+$ cells indeed decreased with increasing time separation between the CFSE and DDAO pulses (Figure 1D), which is consistent with the gradual replacement of the cells present during the initial pulse with newly incorporated cells that are $CFSE^-$ (Figure 1D).

Toward the goal of quantifying the turnover rate in our pulse-chase assays, we combined volume imaging via 3D spinning disk confocal microscopy (necessary due to the curvature of the epidermis) with the establishment of an image analysis pipeline (Figure 1E). The surface extraction tool Premosa was used to generate a 2D representation of the epidermis from 3D volumes,[34] in which individual epidermal cells were subsequently segmented via the deep-learning-based object segmentation method Stardist.[35] This cell segmentation involves model training with image pairs consisting of raw, surface-extracted images and their corresponding manually annotated images (Figure 1F). For model verification, we manually annotated ground-truth labels and compared them to the predictions obtained from the model (Figure 1G; see STAR Methods for details). Using manually annotated ground truths of altogether 27,668 cells, the model achieved a segmentation accuracy above 90% for both $CFSE^+$ and $DDAO^+$ cells of the ventral epidermis (Figure 1H). In the dorsal epidermis, the accuracy of the model also exceeded 90% for CFSE-labeled epidermal cells (Figure 1I), but the detection of cells in the DDAO channel was less reliable (accuracy $\leqq$ 90%). We therefore used the quantification of $DAPI^+$ nuclei in the extracted epidermal layer as an alternative total cell count (accuracy >90%) (Figure 1I). Overall, our analysis pipeline allows the accurate quantification of old and new cells in the planarian epidermis and thus the quantification of the turnover rate.

Using this assay, we first sought to determine the turnover kinetics of the multi-ciliated ventral epidermis, on which planarians rely for their gliding motility.[36–40] Quantifications of the ratio of $CFSE^+/DDAO^+$ cells over time indicated that, on average, 80% of the ventral epidermal cells were replaced within 8 days (Figure 2A). Based on these data, we calculated the ventral epidermal cell half-life (i.e., the time by which 50% of the labeled cells have been replaced) to be 4.5 days (Figure 2C). In pulse-chase experiments on animals 7 days post-lethal irradiation, the decline of the $CFSE^+/DDAO^+$ ratio was much slower and stabilized at 4 days post-CFSE staining (Figure S1). This result is consistent with the known time lag in the depletion of epidermal progenitors after irradiation[18,24] and thus confirms our assumption that the loss of the CFSE label in our assay reflects cell replacement rather than dye leakage. Given the distinct morphological features and patterning signal dependencies of the epidermis in planarians,[39,41–44] we also assayed the turnover rate of the dorsal epidermis. Interestingly, we found that the turnover rate in the dorsal epidermis was much slower than in the

Figure 1. Assay development for quantifying epidermal cell turnover

(A) Schematic of the labeling assay for the quantification of epidermal cell turnover. See the main text for details.

(B) Surface-extracted CFSE pulse-labeled ventral epidermis. Scale bar: 100 μm.

(C) CFSE label in sagittal section. Scale bar: 100 μm.

(D) Representative images demonstrating the gradual loss of $CFSE^+$ cells within the ventral epidermis (DDAO) with increasing chase times (gray: DAPI). dps, days post-CFSE staining. Scale bar: 20 μm.

(E) Schematic visualizing the image analysis procedure. Shown is the ventral epidermis. Scale bar: 100 μm.

(F) Example for manually annotated training data for segmentation model.

(G) Predicted segmentations of $CFSE^+$ cells by the model.

(H and I) Accuracy assessment of the segmentation model in the ventral (H) and dorsal (I) epidermis at indicated time points. An accuracy of 1 corresponds to equal cell counts between automatically and manually segmented images. Data points represent individual fields of view. (H) n = 99 fields; (I) n = 210 fields. Error bar: standard deviation at indicated mean value.

Please cite this article in press as: Lee et al., Epidermal turnover in the planarian *Schmidtea mediterranea* involves basal cell extrusion and intestinal digestion, Cell Reports (2024), https://doi.org/10.1016/j.celrep.2024.114305

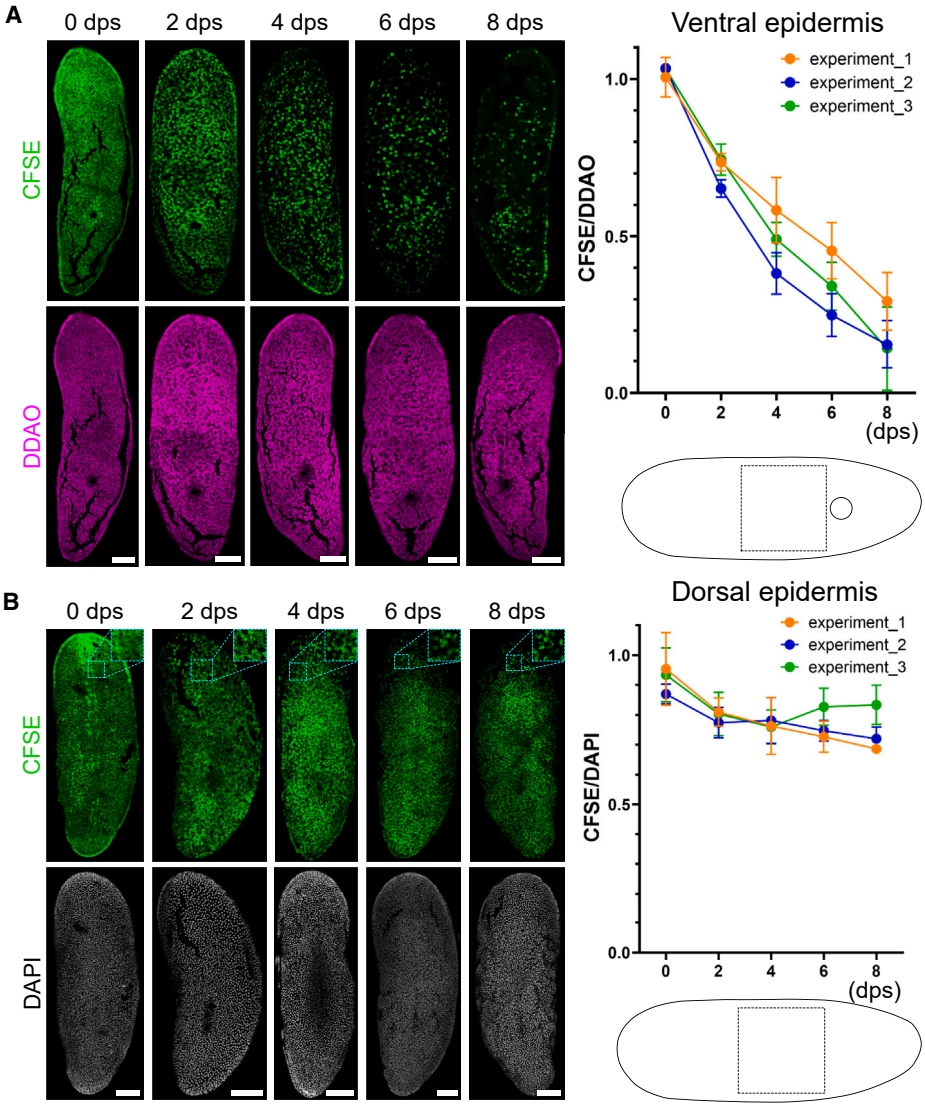

(legend on next page)

Please cite this article in press as: Lee et al., Epidermal turnover in the planarian *Schmidtea mediterranea* involves basal cell extrusion and intestinal digestion, Cell Reports (2024), https://doi.org/10.1016/j.celrep.2024.114305

ventral epidermis, with ~80% of the original cell cohort remaining 8 days after the initial pulse (Figure 2B). A direct comparison of the turnover rates between dorsal and ventral epidermis via linear regression analysis revealed a half-life of ~20 days dorsally as compared to ~4.5 days ventrally (Figure 2C). Our results demonstrate tissue specificity in turnover rates and that the ventral epidermis is a particularly dynamic tissue.

Epidermal cells can undergo either shedding toward the outside (apical extrusion) or delamination toward the inside (basal extrusion). To distinguish between these possibilities, we thought to live image epidermal turnover in the ventral epidermis. Live imaging planarians remains a challenge, and cell dynamics have so far not been visualized. Building on our previous efforts,[45,46] we developed a live-imaging procedure involving the combination of linalool anaesthetization and agarose embedding under a gas-permeable polymethylpentene disc to immobilize the worms. Additionally, low-excitation imaging of far-red live dyes together with denoising was implemented to minimize the strong photosensitivity of planarians[47] (Figure 3A). Specifically, we used the nuclear dye RedDot1 and the cytoplasmic label CellTracker Deep Red, which were both brighter and more photostable than DDAO under our imaging conditions (data not shown). Despite these measures, occasional contractions of the body wall musculature (twitches) still interfered with the intended cell tracking. Further reduction of excitation intensity and exposure times, together with post-acquisition drift correction to correct for residual twitching, enabled the stable tracing of RedDot1-stained epidermal nuclei for up to 2 h (Figure 3B). Content-aware image restoratation driven denoising (CARE)[48] of the noisy image sequence further achieved accurate nuclear detection, enabling long-term tracking and addressing the direction of cell extrusion in the epidermis.

As expected from a terminally differentiated epidermis, the epidermal nuclei in our time-lapse sequences were mostly static. Interestingly, in 7 processed movie sequences, totaling approximately 14 h and 6,000 cells, we never observed the extrusion or shedding of an epidermal nucleus outwards. This was despite the fact that we always set the z range of our image stacks between 6 μm above and 45 μm below the epidermis, with the expectation that such outward displacements would be observed. Instead, we occasionally observed epidermal nuclei undergoing rapid inward movement, traversing a zone largely devoid of nuclei (Figure 3C; Video S1) before encountering more densely populated tissue layers. The inward nuclear movements typically occurred over a vertical distance of ≧15 μm (Figures 3C and 3D). In addition, the intensity of the nuclei increased prior to internalization (Figure 3E), suggesting that epidermal nuclei may undergo nuclear condensation prior to internalization. Live imaging with a cytoplasmic label provided further evidence that the vertical movements represent basal extrusion events with gap closure by the surrounding cells (Video S2). Epidermal cell internalization events were comparatively rare at 1.9 events per 2 h with approximately 860 nuclei per field of view. Overall, our live-imaging experiments suggest that planarian epidermal turnover occurs by basal extrusion and further internalization of epidermal cells.

Given these results, the fate and destination of the internalized epidermal cells became an important question. As a first approach, we used live imaging of epidermal nuclei together with prior feeding of a fluorescent dye to label the intestine as a landmark of deep tissues. We observed that the basally extruded epidermal cells rapidly translocated into close proximity to the gut branches (Figure 4A). The walls of the planarian intestine are largely composed of so-called phagocytes, which are known to actively phagocytose material via their surface.[49–53] The maximum live imaging time of 2 h was insufficient to determine the further fate of internalized nuclei. As an alternative approach, we returned to our CFSE pulse-chase assay and asked whether the CFSE surface label might eventually reach the intestine. Worms fixed immediately after CFSE staining were completely devoid of CFSE fluorescence in all sub-epidermal tissues, confirming the epidermal specificity of the labeling strategy (Figure 4B). However, 4 days post-CFSE staining, $CFSE^+$ objects partially colocalized with phagocytosed CellTracker Deep Red delivered by feeding 1 day prior to fixation (Figure 4B). Moreover, quantifications of the $CFSE^+$ object density within the volume occupied by the CellTracker Deep Red label versus the mesenchyme indicated that the epidermis-derived structures specifically accumulate within gut branches (Figures 4C and 4D). To unambiguously demonstrate the accumulation of $CFSE^+$ structures within phagocytes, we combined the CFSE pulse-chase assay and *in situ* hybridization with a phagocyte-specific probe (*dd_Smed_v6*: *dd_75*[54]). As shown in Figure 4E, $CFSE^+$ structures were detected within the cytoplasm of phagocytes after 4 days of chase but not immediately after labeling. Taken together, our results suggest that epidermal cells are continuously internalized to accumulate in intestinal phagocytes.

This raises the possibility that phagocytes may catabolize not only ingested food but also endogenous cells undergoing turnover. Accordingly, $CFSE^+$ remnants of internalized epidermal cells should accumulate in phagocytes under experimental conditions that interfere with their digestive processes. We therefore treated planarians with the lysosome inhibitor chloroquine, which blocks intracellular digestion by interfering with the acidification of late endosomal compartments.[55,56] We found that planarians can survive more than 2 weeks of chloroquine treatment without overt morphological changes in the intestine (Figures S2A and S2B). Interestingly, we found that chloroquine exposure indeed strongly increased both the volume and the density of intestinal $CFSE^+$ objects above controls (Figures 4F–4H). Both observations are consistent with reduced digestion of phagosomal contents in the presence of chloroquine. Furthermore, chloroquine treatment also increased the relative volume of $CFSE^+$ objects in the mesenchyme 4 days after CFSE treatment (Figure S3) compared to control samples, suggesting that

Figure 2. Quantification of epidermal turnover kinetics

(A and B) Visualization (left) and quantification (right) of cell turnover rates in the ventral (A) and dorsal (B) epidermis in the boxed body region. n = 3 independent replicates (3–10 specimens/time point/experiment). Error bars denote standard deviation. Scale bars: 100 μm.

(C) Linear regression analysis of the turnover rates in ventral and dorsal epidermis. Dashed lines: 95% confidence intervals.

Please cite this article in press as: Lee et al., Epidermal turnover in the planarian *Schmidtea mediterranea* involves basal cell extrusion and intestinal digestion, Cell Reports (2024), https://doi.org/10.1016/j.celrep.2024.114305

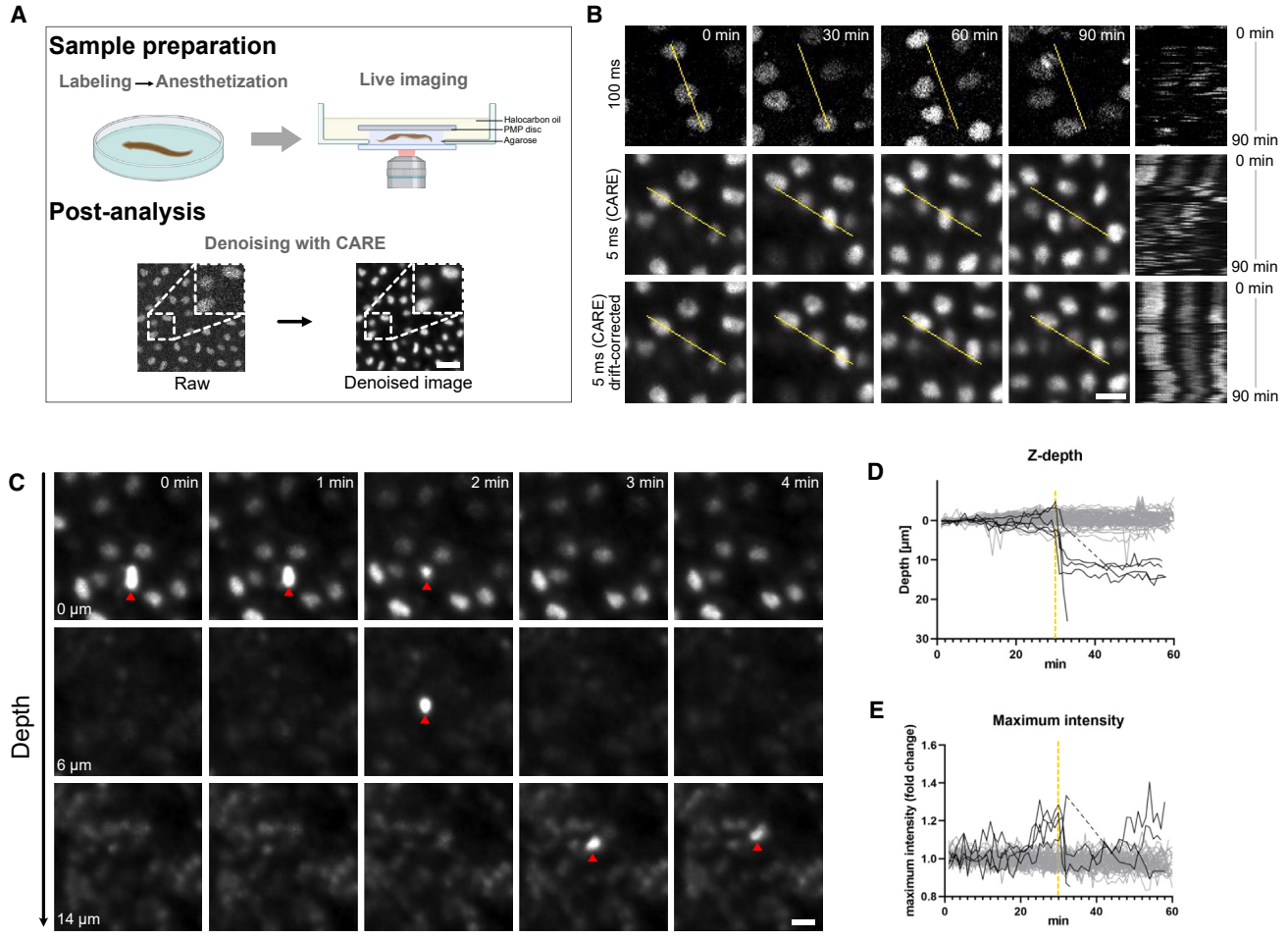

Figure 3. Live imaging of epidermal cell extrusion

(A) Schematic of the developed live-imaging procedure including sample preparation, mounting, and image denoising. Scale bar: 20 µm. Schematics were created with BioRender.com

(B) Processing of raw imaging data by CARE-mediated denoising and 3D drift correction to compensate for tissue twitching. Kymographs (right column) at indicated yellow lines visualize the optimization effects. Scale bar: 10 µm.

(C) Internalization of a RedDot1-labeled ventral epidermal nucleus. Frames are confocal sections at the indicated time points and z depths. The red triangle highlights the internalizing nucleus. Scale bar: 10 µm.

(D and E) Quantification of the relative z depth (D) and maximum pixel intensity (E) of ventral epidermal nuclei. Solid black lines refer to internalizing epidermal nuclei and gray lines to residing epidermal nuclei. Dashed black lines indicate manually connected tracks. The yellow dashed lines indicate time of internalization. Data in (D) were quantified from 5 movies from 4 different individuals. The data in (E) were quantified from 4 movies from 3 different individuals.

chloroquine may additionally affect the uptake of internalized epidermal cells into phagocytes. In conclusion, our results identify the digestion of internalized epithelial cells by intestinal phagocytes as the last stage of the complex turnover of the planarian epidermis.

DISCUSSION

Using pulse-chase and live-imaging assays, here we investigate the kinetics and physiological mechanisms of cell turnover in the planarian epidermis. We find that turnover rates differ significantly between the dorsal and ventral epidermis, the latter being a highly dynamic tissue. Surprisingly, cell turnover in the ventral epidermis is mediated by cell internalization rather than shedding. As illustrated in Figure 4I, our results collectively show that epidermal cells undergo a "march of death" that involves crossing the thick basement membrane beneath the epidermis, the body wall musculature, and a section of the mesenchyme to be phagocytosed and eventually digested by the phagocytes that make up the walls of the intestine. This process not only represents an unusually complex sequence of events for cell clearance but also reverses the outward migration that every epidermal progenitor undergoes after its "birth" in an asymmetric cell division of a pluripotent neoblast situated within the mesenchyme.[18,24,25,57] With long-range cell migration as part of both cell birth and death, our results add another element to the extraordinarily dynamic tissue architecture of planarians.

Please cite this article in press as: Lee et al., Epidermal turnover in the planarian *Schmidtea mediterranea* involves basal cell extrusion and intestinal digestion, Cell Reports (2024), https://doi.org/10.1016/j.celrep.2024.114305

CellPress
OPEN ACCESS

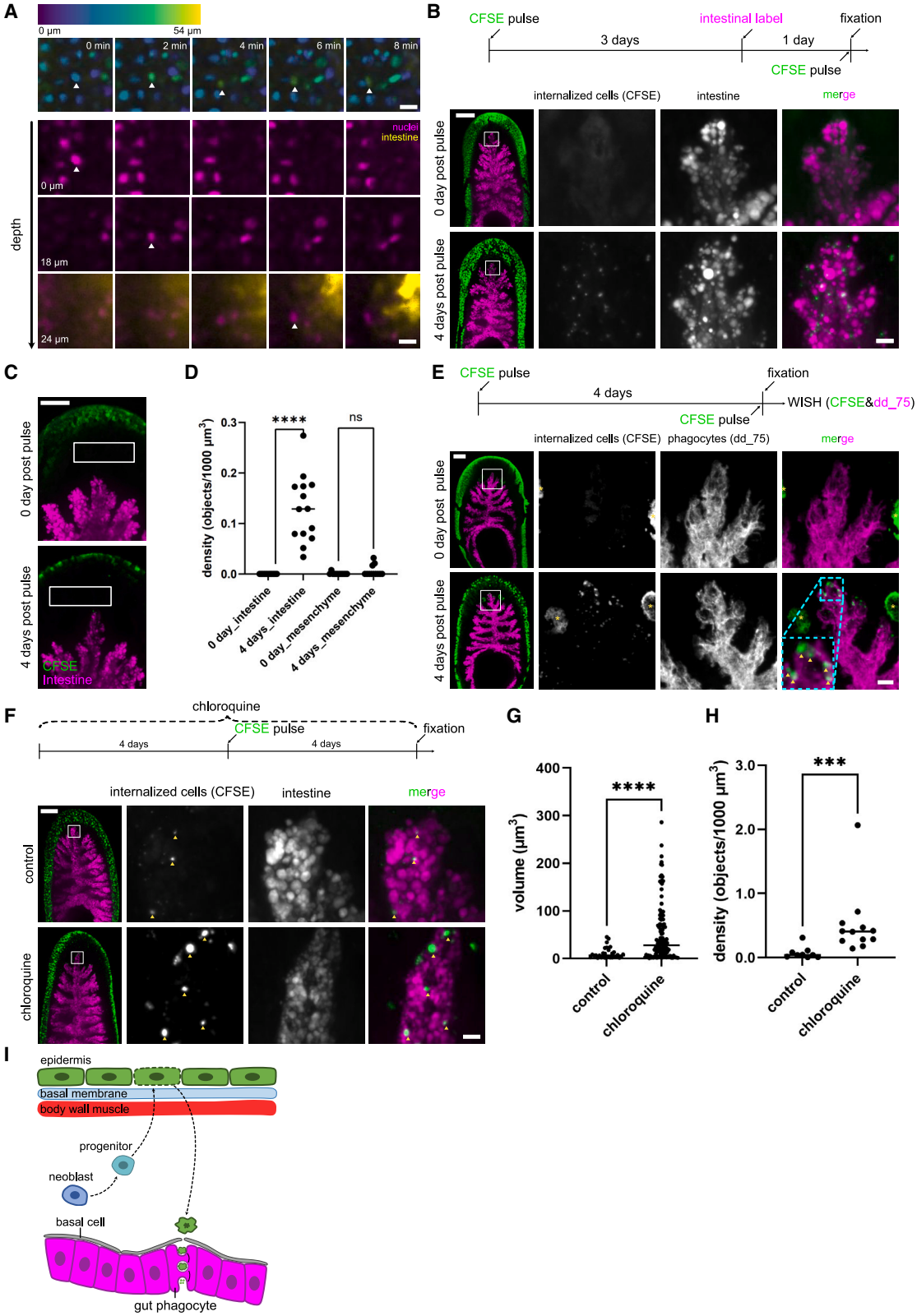

(legend on next page)

Please cite this article in press as: Lee et al., Epidermal turnover in the planarian *Schmidtea mediterranea* involves basal cell extrusion and intestinal digestion, Cell Reports (2024), https://doi.org/10.1016/j.celrep.2024.114305

Our pulse-chase epidermal turnover quantifications predict an hourly internalization probability of 1 in 215 cells, assuming desynchronized and stochastic steady-state turnover. However, the internalization frequency we observed in our in live recordings was ~4 times lower. Furthermore, we never observed new cell integration in any of our time-lapse sequences, which should occur at approximately the same frequency as internalization events at steady state. Possible explanations for this discrepancy could include anaesthetization, dye labeling side effects, or adverse effects of our imaging conditions. Nevertheless, the combination of internalization as the only observed turnover mode of epidermal cells (Figure 3C), the live tracing of individual nuclei down to the vicinity of intestinal branches (Figure 4A), the delayed appearance of the covalent CFSE surface label in intestinal phagocytes (Figure 4B), and the effects of chloroquine treatment (Figures 4F–4H) collectively support the digestion of internalized epidermal cells in intestinal phagocytes.

Interestingly, a recent study demonstrated that light-induced depigmentation in planarians[58] also involves the translocation of damaged pigment cell remnants to the intestine and their uptake into phagocytes via phagocytosis.[59] Together with our data, these findings therefore demonstrate that the intestine mediates the clearance of multiple cell types, both under pathological challenges[59] and at steady state (our data). This mode of cell clearance is unusually elaborate in comparison with clearing mechanisms in other model systems, especially for epidermal cells. Most animal epithelia shed cells toward the outside, with the constitutive shedding of vertebrate intestinal epithelium cells at the cristae tip[60–62] or the apical extrusion of epidermal cells in the tail of developing zebrafish[63] as examples. Although basal extrusion is also known to exist in other systems,[8,64,65] it is frequently associated with pathologies and consequent metastasis formation.[66–68] The crossing of the collagen-rich basement membrane[69–71] that planarian epidermal cells undertake post-basal extrusion establishes an interesting conceptual parallel to metastasis formation in vertebrates but also raises a question regarding the eventual purpose of the unusually elaborate cell clearance mechanism in planarians.

An interesting possibility is that the self-catabolism of cells may ultimately serve as an energy-recovery mechanism. Planarians never reach a stable body size. They grow when fed, but shrink during periods of starvation, gradually reducing their total number of cells.[22,23] The starvation response is termed degrowth, and it has long been speculated that self-catabolism contributes to the energy budget of planarians during starvation. The faster degrowth rate of chloroquine-treated worms that we observed is consistent with this hypothesis (Figures S2C and S2D), but whether the death of the animals on ~day 16 after the start of chloroquine treatment is due to toxic side effects or the depletion of the organism's energy stores needs to be addressed in future studies. The above quantitative considerations further illustrate that even the self-catabolism of one of the most short-lived cell types results in a comparatively low retrograde cell flow at steady state. In addition, the flat body architecture of planarians and their branched intestine mean that even epidermal cells, as the most peripheral cell type, have to travel a maximum of <100 μm to reach the nearest intestinal branch, well within range of cell migrations in other systems[8,72] and highlighting the dual benefit of intestinal branching for nutrient distribution and efficient cell recycling. Overall, these considerations make intestinal digestion as a general feature of planarian cell turnover a plausible proposition.

Some of the interesting questions raised by our study include whether the transfer to the intestine reflects the autonomous migration of internalizing cells or the less parsimonious transfer via a migratory cell type (e.g., phagocytes) and the nature of the guidance cues or tracks that facilitate the inward movement toward the intestine (e.g., dorsal/ventral muscle fibers). Also unknown are the triggering mechanisms that initiate basal extrusion and ultimately determine the specific half-lives of ventral and dorsal epidermal cells (Figures 2 and 3C). In *Drosophila*, basal extrusion from the amnioserosa or the larval epidermis requires the partial activation of apoptosis.[65,73–76] The concomitant brightness increase of epidermal nuclei prior to internalization (Figure 3E) and the light-induced appearance of TUNEL$^+$ cells at the site of pigment cells[58,59] indicate that the partial activation of apoptotic processes may also initiate self-clearance in planarians. Similarly, the validation of intestinal digestion as a clearance mechanism for other tissues and organs, the measurement of tissue/organ-specific turnover rates, and the quantification of their

Figure 4. Tracing the fate of basally extruded epidermal cells

(A) Two-color time-lapse imaging of RedDot1-labeled ventral epidermal cells and CellTracker Red CMTPX-labeled intestinal cells. Top row: maximum projected, depth color-coded 3D time-lapse recordings of ventral epidermis nuclei. Rows below: single-plane time-lapse recordings of epidermal nuclei and intestine at the indicated z depth. White arrowheads: internalizing cell. Scale bar: 10 μm.

(B) CFSE surface label chase into the intestine. Top: experimental procedure. Bottom: maximum-projected images. Scale bar overview image: 100 μm. Scale bar detail image: 10 μm.

(C) Lack of CFSE signal accumulation in the mesenchyme (boxed) under the same condition as in (B). Scale bar: 50 μm.

(D) Quantification of CFSE$^+$ object density in the intestine and mesenchyme at indicated chase periods. Data points correspond to individual specimens. n = 14 for 4 day_intestine; n = 12 for every other condition. Horizontal lines indicate median values. ****$p < 0.0001$ (Mann-Whitney U test); ns, non-significant.

(E) Visualization of CFSE accumulation (anti-fluorescein staining) in the intestine (phagocyte marker *dd_Smed_v6*: *dd_75 in situ* hybridization). Yellow arrowheads: CFSE$^+$ objects. Shown are maximum intensity projections. An asterisk (*) indicates background signal from photoreceptors. Scale bars: 100 μm (overviews) and 20 μm (details).

(F) Assessment of intestinal CFSE signal accumulation (yellow arrowheads) in the presence of the lysosome inhibitor chloroquine. All images are maximum projections. Scale bars, 100 μm (left) and 10 μm (detail).

(G and H) Quantifications of intestinal CFSE$^+$ object volumes (G) and density (H). n = 9 individuals for control, n = 12 for chloroquine treatments. Solid circles indicate individual CFSE$^+$ objects in (G) or the overall density within one sample in (H). Horizontal lines represent the median. ****$p << 0.0001$ and ***$p < 0.001$ (Mann-Whitney U test).

(I) Model of epidermal turnover in planarians.

Table 1. Primer pairs used for probe generation

Gene name	Fw primers	Re primers
dd_Smed_v6: dd_75	CATTACCATCCCGTCGGATC CACTAGTAACGTGTGTT GCGGTCGTTTATT	CCAATTCTACCCGTAGAAGGCACAGTCGA GGAATATCGCATCCTGCCACAG
dd_Smed_v6: dd_115	CATTACCATCCCGTCGGATCCA CTAGTAACGCAGGGCAG AATAACAATTTTGA	CCAATTCTACCCGTAGAAGGCACAGTCGAG GCGAGTTCTAAGTCATCAATCA

Underlined nucleotides represent the overhangs for insertion into the pPR-T4P vector cloning site. Fw, forward; Re, reverse.

dependence on the energy status of the organism are important questions for future research. Of note, live-imaging approaches in general will be important for understanding planarian tissue dynamics. Our study provides an important proof of principle in this respect, and the approaches we have developed are a starting point for the systematic investigation of this dynamic dimension of planarian biology.

Limitations of the study

Our quantification of epidermal turnover rates using the CFSE/DDAO labeling assay assumes steady-state dynamics and may underestimate the half-life of epidermal cells when the tissue is growing (adding cells). The discrepancy between measured internalization rates and expectations based on our half-life measurements leaves open the possibility that processes other than internalization may contribute or that internalization rates are affected by our imaging conditions. The lack of observations of cell integration events in the epidermis is another indication that the current live-imaging protocol may affect tissue dynamics. Similarly, the current limitation of 2–3 h of live-imaging time did not allow direct visualization of how internalized epidermal cells entered the intestine, meaning that both direct phagocytosis from the mesenchymal side and paracellular passage into the lumen prior to phagocytosis remain possible uptake routes. Due to the current lack of transgenic reporter expression tools in planarians, our live-imaging efforts remain limited to vital dyes and do not allow, for example, the tracking of membrane-labeled epithelial cells to investigate the mode and mechanisms of cell migration toward the gut. Overall, our study highlights the need for further concerted development of both live-imaging approaches and labeling strategies to study planarian tissue dynamics.

STAR★METHODS

Detailed methods are provided in the online version of this paper and include the following:

- KEY RESOURCES TABLE
- RESOURCES AVAILABILITY
  - Lead contact
  - Materials availability
  - Data and code availability
- EXPERIMENTAL MODEL AND STUDY PARTICIPANT DETAILS
- METHOD DETAILS
  - X-Ray irradiation
  - Cloning and probe synthesis
  - Whole-mount *in situ* hybridization
  - CFSE and DDAO labeling of the epidermis
  - Sample preparation for live-imaging
  - Microscopy
  - Visualization of time-series images
  - Premosa surface extraction
  - Stardist model training
  - Stardist model verification
  - CARE model training
  - Drug treatment
  - Image analysis and statistical analysis

SUPPLEMENTAL INFORMATION

Supplemental information can be found online at https://doi.org/10.1016/j.celrep.2024.114305.

ACKNOWLEDGMENTS

We thank Ludwik Gąsiorowski for his critical reading of the manuscript draft and Stefen Werner for fruitful discussions. We thank R. Kluiver, J. Krull, and the MPI-NAT animal caretakers for worm care support. We want to thank Sarah Mansour for pilot experiments leading to the establishement of the pulse-chase assay. This work was supported by the Max Planck Society and the Behrens-Weise-Foundation.

AUTHOR CONTRIBUTIONS

J.-R.L., T.B., and J.C.R. conceptualized the project and designed the experiments. J.-R.L., T.B., and C.M. conducted the experiments. J.-R.L. and T.B. analyzed the results. T.B. provided the technical support for the image analysis methods. A.T. made the initial observation of internalizing epithelial cells. J.-R.L., T.B., and J.C.R. wrote the manuscript.

DECLARATION OF INTERESTS

The authors declare no competing interests.

Received: November 6, 2023
Revised: March 21, 2024
Accepted: May 15, 2024
Published: June 20, 2024

REFERENCES

1. Barker, N. (2014). Adult intestinal stem cells: critical drivers of epithelial homeostasis and regeneration. Nat Rev Mol Cell Bio *15*, 19–33. https://doi.org/10.1038/nrm3721.
2. Crosnier, C., Stamataki, D., and Lewis, J. (2006). Organizing cell renewal in the intestine: stem cells, signals and combinatorial control. Nat. Rev. Genet. *7*, 349–359. https://doi.org/10.1038/nrg1840.
3. Beumer, J., and Clevers, H. (2021). Cell fate specification and differentiation in the adult mammalian intestine. Nat. Rev. Mol. Cell Biol. *22*, 39–53. https://doi.org/10.1038/s41580-020-0278-0.
4. Tetteh, P.W., Basak, O., Farin, H.F., Wiebrands, K., Kretzschmar, K., Begthel, H., van den Born, M., Korving, J., de Sauvage, F., van Es, J.H., et al. (2016). Replacement of Lost Lgr5-Positive Stem Cells through

Plasticity of Their Enterocyte-Lineage Daughters. Cell Stem Cell *18*, 203–213. https://doi.org/10.1016/j.stem.2016.01.001.

5. Dini, L., Lentini, A., Diez, G.D., Rocha, M., Falasca, L., Serafino, L., and Vidalvanaclocha, F. (1995). Phagocytosis of Apoptotic Bodies by Liver Endothelial-Cells. J. Cell Sci. *108*, 967–973. https://doi.org/10.1242/jcs.108.3.967.
6. Dini, L., Pagliara, P., and Carlà, E.C. (2002). Phagocytosis of apoptotic cells by liver: A morphological study. Microsc. Res. Tech. *57*, 530–540. https://doi.org/10.1002/jemt.10107.
7. Hoijman, E., Hakkinen, H.M., Tolosa-Ramon, Q., Jimenez-Delgado, S., Wyatt, C., Miret-Cuesta, M., Irimia, M., Callan-Jones, A., Wieser, S., and Ruprecht, V. (2021). Cooperative epithelial phagocytosis enables error correction in the early embryo. Nature *590*, 618–623. https://doi.org/10.1038/s41586-021-03200-3.
8. Ninov, N., Chiarelli, D.A., and Martín-Blanco, E. (2007). Extrinsic and intrinsic mechanisms directing epithelial cell sheet replacement during Drosophila metamorphosis. Development *134*, 367–379. https://doi.org/10.1242/dev.02728.
9. Nagata, S., Hanayama, R., and Kawane, K. (2010). Autoimmunity and the Clearance of Dead Cells. Cell *140*, 619–630. https://doi.org/10.1016/j.cell.2010.02.014.
10. Savill, J., Dransfield, I., Gregory, C., and Haslett, C. (2002). A blast from the past: Clearance of apoptotic cells regulates immune responses. Nat. Rev. Immunol. *2*, 965–975. https://doi.org/10.1038/nri957.
11. Munoz, L.E., Lauber, K., Schiller, M., Manfredi, A.A., and Herrmann, M. (2010). The role of defective clearance of apoptotic cells in systemic autoimmunity. Nat. Rev. Rheumatol. *6*, 280–289. https://doi.org/10.1038/nrrheum.2010.46.
12. Rink, J.C. (2018). Stem Cells, Patterning and Regeneration in Planarians: Self-Organization at the Organismal Scale. Methods Mol. Biol. *1774*, 57–172. https://doi.org/10.1007/978-1-4939-7802-1_2.
13. Reddien, P.W. (2018). The Cellular and Molecular Basis for Planarian Regeneration. Cell *175*, 327–345. https://doi.org/10.1016/j.cell.2018.09.021.
14. Cebria, F., Adell, T., and Salo, E. (2018). Rebuilding a planarian: from early signaling to final shape. Int. J. Dev. Biol. *62*, 537–550. https://doi.org/10.1387/ijdb.180042es.
15. Shibata, N., Rouhana, L., and Agata, K. (2010). Cellular and molecular dissection of pluripotent adult somatic stem cells in planarians. Dev. Growth Differ. *52*, 27–41. https://doi.org/10.1111/j.1440-169X.2009.01155.x.
16. Baguñà, J. (2012). The planarian neoblast: the rambling history of its origin and some current black boxes. Int. J. Dev. Biol. *56*, 19–37. https://doi.org/10.1387/ijdb.113463jb.
17. Baguna, J., Salo, E., and Auladell, C. (1989). Regeneration and pattern formation in planarians: III. Evidence that neoblasts are totipotent stem cells and the source of blastema cells. Development *107*, 77–86. https://doi.org/10.1242/dev.107.1.77.
18. Eisenhoffer, G.T., Kang, H., and Sánchez Alvarado, A. (2008). Molecular analysis of stem cells and their descendants during cell turnover and regeneration in the planarian Schmidtea mediterranea. Cell Stem Cell *3*, 327–339. https://doi.org/10.1016/j.stem.2008.07.002.
19. Atabay, K.D., LoCascio, S.A., de Hoog, T., and Reddien, P.W. (2018). Self-organization and progenitor targeting generate stable patterns in planarian regeneration. Science *360*, 404–409. https://doi.org/10.1126/science.aap8179.
20. Reddien, P.W. (2021). Principles of regeneration revealed by the planarian eye. Curr. Opin. Cell Biol. *73*, 19–25. https://doi.org/10.1016/j.ceb.2021.05.001.
21. Wagner, D.E., Wang, I.E., and Reddien, P.W. (2011). Clonogenic Neoblasts Are Pluripotent Adult Stem Cells That Underlie Planarian Regeneration. Science *332*, 811–816. https://doi.org/10.1126/science.1203983.
22. Baguna, J., and Romero, R. (1981). Quantitative Analysis of Cell Types during Growth, Degrowth and Regeneration in the Planarians Dugesia mediterranea and Dugesia tigrina. Hydrobiologia *84*, 181–194. https://doi.org/10.1007/Bf00026179.
23. Thommen, A., Werner, S., Frank, O., Philipp, J., Knittelfelder, O., Quek, Y., Fahmy, K., Shevchenko, A., Friedrich, B.M., Jülicher, F., and Rink, J.C. (2019). Body size-dependent energy storage causes Kleiber's law scaling of the metabolic rate in planarians. Elife *8*, e38187. https://doi.org/10.7554/eLife.38187.
24. Tu, K.C., Cheng, L.C., Vu, H.T.K., Lange, J.J., McKinney, S.A., Seidel, C.W., and Alvarado, A.S. (2015). Egr-5 is a post-mitotic regulator of planarian epidermal differentiation. Elife *4*, e10501. https://doi.org/10.7554/eLife.10501.
25. van Wolfswinkel, J.C., Wagner, D.E., and Reddien, P.W. (2014). Single-cell analysis reveals functionally distinct classes within the planarian stem cell compartment. Cell Stem Cell *15*, 326–339. https://doi.org/10.1016/j.stem.2014.06.007.
26. Zhu, S.J., Hallows, S.E., Currie, K.W., Xu, C., and Pearson, B.J. (2015). A mex3 homolog is required for differentiation during planarian stem cell lineage development. Elife *4*, e07025. https://doi.org/10.7554/eLife.07025.
27. Zhu, S.J., and Pearson, B.J. (2018). Smed-myb-1 Specifies Early Temporal Identity during Planarian Epidermal Differentiation. Cell Rep. *25*, 38–46.e3. https://doi.org/10.1016/j.celrep.2018.09.011.
28. Baguna, J. (1974). Dramatic mitotic response in planarians after feeding, and a hypothesis for the control mechanism. J. Exp. Zool. *190*, 117–122. https://doi.org/10.1002/jez.1401900111.
29. Wenemoser, D., Lapan, S.W., Wilkinson, A.W., Bell, G.W., and Reddien, P.W. (2012). A molecular wound response program associated with regeneration initiation in planarians. Genes Dev. *26*, 988–1002. https://doi.org/10.1101/gad.187377.112.
30. Pellettieri, J., Fitzgerald, P., Watanabe, S., Mancuso, J., Green, D.R., and Sánchez Alvarado, A. (2010). Cell death and tissue remodeling in planarian regeneration. Dev. Biol. *338*, 76–85. https://doi.org/10.1016/j.ydbio.2009.09.015.
31. Gonzalez-Estevez, C., and Salo, E. (2010). Autophagy and apoptosis in planarians. Apoptosis *15*, 279–292. https://doi.org/10.1007/s10495-009-0445-4.
32. Reddien, P.W., Oviedo, N.J., Jennings, J.R., Jenkin, J.C., and Sánchez Alvarado, A. (2005). SMEDWI-2 is a PIWI-like protein that regulates planarian stem cells. Science *310*, 1327–1330. https://doi.org/10.1126/science.1116110.
33. Newmark, P.A., and Sánchez Alvarado, A. (2000). Bromodeoxyuridine specifically labels the regenerative stem cells of planarians. Dev. Biol. *220*, 142–153. https://doi.org/10.1006/dbio.2000.9645.
34. Blasse, C., Saalfeld, S., Etournay, R., Sagner, A., Eaton, S., and Myers, E.W. (2017). PreMosa: extracting 2D surfaces from 3D microscopy mosaics. Bioinformatics *33*, 2563–2569. https://doi.org/10.1093/bioinformatics/btx195.
35. Schmidt, U., Weigert, M., Broaddus, C., and Myers, G. (2018). Cell Detection with Star-Convex Polygons. Lect Notes Comput Sc *11071*, 265–273. https://doi.org/10.1007/978-3-030-00934-2_30.
36. Vu, H.T.K., Mansour, S., Kucken, M., Blasse, C., Basquin, C., Azimzadeh, J., Myers, E.W., Brusch, L., and Rink, J.C. (2019). Dynamic Polarization of the Multiciliated Planarian Epidermis between Body Plan Landmarks. Dev. Cell *51*, 526–542.e526. https://doi.org/10.1016/j.devcel.2019.10.022.
37. Azimzadeh, J., Wong, M.L., Downhour, D.M., Sánchez Alvarado, A., and Marshall, W.F. (2012). Centrosome loss in the evolution of planarians. Science *335*, 461–463. https://doi.org/10.1126/science.1214457.
38. Rompolas, P., Azimzadeh, J., Marshall, W.F., and King, S.M. (2013). Analysis of ciliary assembly and function in planaria. Methods Enzymol. *525*, 245–264. https://doi.org/10.1016/B978-0-12-397944-5.00012-2.

39. Rompolas, P., Patel-King, R.S., and King, S.M. (2010). An Outer Arm Dynein Conformational Switch Is Required for Metachronal Synchrony of Motile Cilia in Planaria. Mol. Biol. Cell *21*, 3669–3679. https://doi.org/10.1091/mbc.E10-04-0373.

40. Rompolas, P., Patel-King, R.S., and King, S.M. (2009). Schmidtea mediterranea: a model system for analysis of motile cilia. Methods Cell Biol. *93*, 81–98. https://doi.org/10.1016/S0091-679X(08)93004-1.

41. Kato, K., Orii, H., Watanabe, K., and Agata, K. (2001). Dorsal and ventral positional cues required for the onset of planarian regeneration may reside in differentiated cells. Dev. Biol. *233*, 109–121. https://doi.org/10.1006/dbio.2001.0226.

42. Molina, M.D., Saló, E., and Cebrià, F. (2007). The BMP pathway is essential for re-specification and maintenance of the dorsoventral axis in regenerating and intact planarians. Dev. Biol. *311*, 79–94. https://doi.org/10.1016/j.ydbio.2007.08.019.

43. Reddien, P.W., Bermange, A.L., Kicza, A.M., and Sánchez Alvarado, A. (2007). BMP signaling regulates the dorsal planarian midline and is needed for asymmetric regeneration. Development *134*, 4043–4051. https://doi.org/10.1242/dev.007138.

44. Wurtzel, O., Oderberg, I.M., and Reddien, P.W. (2017). Planarian Epidermal Stem Cells Respond to Positional Cues to Promote Cell-Type Diversity. Dev. Cell *40*, 491–504.e5. https://doi.org/10.1016/j.devcel.2017.02.008.

45. Boothe, T., Hilbert, L., Heide, M., Berninger, L., Huttner, W.B., Zaburdaev, V., Vastenhouw, N.L., Myers, E.W., Drechsel, D.N., and Rink, J.C. (2017). A tunable refractive index matching medium for live imaging cells, tissues and model organisms. Elife *6*, e27240. https://doi.org/10.7554/eLife.27240.

46. Boothe, T., Ivankovic, M., Grohme, M.A., Markus, M.A., Dullin, C., Xu, X.B., and Rink, J.C. (2023). Content aware image restoration improves spatio-temporal resolution in luminescence imaging. Commun. Biol. *6*, 518. https://doi.org/10.1038/s42003-023-04886-z.

47. Shettigar, N., Joshi, A., Dalmeida, R., Gopalkrishna, R., Chakravarthy, A., Patnaik, S., Mathew, M., Palakodeti, D., and Gulyani, A. (2017). Hierarchies in light sensing and dynamic interactions between ocular and extra-ocular sensory networks in a flatworm. Sci. Adv. *3*, e1603025. https://doi.org/10.1126/sciadv.1603025.

48. Weigert, M., Schmidt, U., Boothe, T., Müller, A., Dibrov, A., Jain, A., Wilhelm, B., Schmidt, D., Broaddus, C., Culley, S., et al. (2018). Content-aware image restoration: pushing the limits of fluorescence microscopy. Nat. Methods *15*, 1090–1097. https://doi.org/10.1038/s41592-018-0216-7.

49. Ishii, S., and Sakurai, T. (1991). Food Ingestion by Planarian Intestinal Phagocytic-Cells - a Study by Scanning Electron-Microscopy. Hydrobiologia *227*, 179–185. https://doi.org/10.1007/Bf00027600.

50. Willier, B.H., Hyman, L.H., and Rifenburgh, S.A. (1925). A histochemical study of intracellular digestion in triclad flatworms. J. Morphol. *40*, 299–340. https://doi.org/10.1002/jmor.1050400205.

51. Forsthoefel, D.J., Cejda, N.I., Khan, U.W., and Newmark, P.A. (2020). Cell-type diversity and regionalized gene expression in the planarian intestine. Elife *9*, e52613. https://doi.org/10.7554/eLife.52613.

52. Forsthoefel, D.J., James, N.P., Escobar, D.J., Stary, J.M., Vieira, A.P., Waters, F.A., and Newmark, P.A. (2012). An RNAi screen reveals intestinal regulators of branching morphogenesis, differentiation, and stem cell proliferation in planarians. Dev. Cell *23*, 691–704. https://doi.org/10.1016/j.devcel.2012.09.008.

53. Forsthoefel, D.J., Park, A.E., and Newmark, P.A. (2011). Stem cell-based growth, regeneration, and remodeling of the planarian intestine. Dev. Biol. *356*, 445–459. https://doi.org/10.1016/j.ydbio.2011.05.669.

54. Fincher, C.T., Wurtzel, O., de Hoog, T., Kravarik, K.M., and Reddien, P.W. (2018). Cell type transcriptome atlas for the planarian Schmidtea mediterranea. Science *360*, eaaq1736. https://doi.org/10.1126/science.aaq1736.

55. Homewood, C.A., Warhurst, D.C., Peters, W., and Baggaley, V.C. (1972). Lysosomes, pH and the anti-malarial action of chloroquine. Nature *235*, 50–52. https://doi.org/10.1038/235050a0.

56. Halcrow, P.W., Geiger, J.D., and Chen, X. (2021). Overcoming Chemoresistance: Altering pH of Cellular Compartments by Chloroquine and Hydroxychloroquine. Front. Cell Dev. Biol. *9*, 627639. https://doi.org/10.3389/fcell.2021.627639.

57. Park, C., Owusu-Boaitey, K.E., Valdes, G.M., and Reddien, P.W. (2023). Fate specification is spatially intermingled across planarian stem cells. Nat. Commun. *14*, 7422. https://doi.org/10.1038/s41467-023-43267-2.

58. Stubenhaus, B.M., Dustin, J.P., Neverett, E.R., Beaudry, M.S., Nadeau, L.E., Burk-McCoy, E., He, X., Pearson, B.J., and Pellettieri, J. (2016). Light-induced depigmentation in planarians models the pathophysiology of acute porphyrias. Elife *5*, e14175. https://doi.org/10.7554/eLife.14175.

59. Lindsay-Mosher, N., Lusk, S., and Pearson, B.J. (2024). Planarians require ced-12/elmo-1 to clear dead cells by excretion through the gut. Cell Rep. *43*, 113621. https://doi.org/10.1016/j.celrep.2023.113621.

60. Potten, C.S. (1992). The Significance of Spontaneous and Induced Apoptosis in the Gastrointestinal-Tract of Mice. Cancer Metast Rev *11*, 179–195. https://doi.org/10.1007/Bf00048063.

61. Potten, C.S. (1997). Epithelial cell growth and differentiation. II. Intestinal apoptosis. Am. J. Physiol. *273*, G253–G257. https://doi.org/10.1152/ajpgi.1997.273.2.G253.

62. Heath, J.P. (1996). Epithelial cell migration in the intestine. Cell Biol. Int. *20*, 139–146. https://doi.org/10.1006/cbir.1996.0018.

63. Eisenhoffer, G.T., Loftus, P.D., Yoshigi, M., Otsuna, H., Chien, C.B., Morcos, P.A., and Rosenblatt, J. (2012). Crowding induces live cell extrusion to maintain homeostatic cell numbers in epithelia. Nature *484*, 546–549. https://doi.org/10.1038/nature10999.

64. Pastor-Pareja, J.C., Grawe, F., Martín-Blanco, E., and García-Bellido, A. (2004). Invasive cell behavior during Drosophila imaginal disc eversion is mediated by the JNK signaling cascade. Dev. Cell *7*, 387–399. https://doi.org/10.1016/j.devcel.2004.07.022.

65. Toyama, Y., Peralta, X.G., Wells, A.R., Kiehart, D.P., and Edwards, G.S. (2008). Apoptotic force and tissue dynamics during Drosophila embryogenesis. Science *321*, 1683–1686. https://doi.org/10.1126/science.1157052.

66. Marshall, T.W., Lloyd, I.E., Delalande, J.M., Näthke, I., and Rosenblatt, J. (2011). The tumor suppressor adenomatous polyposis coli controls the direction in which a cell extrudes from an epithelium. Mol. Biol. Cell *22*, 3962–3970. https://doi.org/10.1091/mbc.E11-05-0469.

67. Slattum, G., Gu, Y., Sabbadini, R., and Rosenblatt, J. (2014). Autophagy in Oncogenic K-Ras Promotes Basal Extrusion of Epithelial Cells by Degrading S1P. Curr. Biol. *24*, 19–28. https://doi.org/10.1016/j.cub.2013.11.029.

68. Slattum, G.M., and Rosenblatt, J. (2014). Tumour cell invasion: an emerging role for basal epithelial cell extrusion. Nat. Rev. Cancer *14*, 495–501. https://doi.org/10.1038/nrc3767.

69. Hori, I. (1979). Structure and regeneration of the planarian basal lamina: an ultrastructural study. Tissue Cell *11*, 611–621. https://doi.org/10.1016/0040-8166(79)90018-1.

70. Chan, A., Ma, S., Pearson, B.J., and Chan, D. (2021). Collagen IV differentially regulates planarian stem cell potency and lineage progression. Proc. Natl. Acad. Sci. USA *118*, e2021251118. https://doi.org/10.1073/pnas.2021251118.

71. Cote, L.E., Simental, E., and Reddien, P.W. (2019). Muscle functions as a connective tissue and source of extracellular matrix in planarians. Nat. Commun. *10*, 1592. https://doi.org/10.1038/s41467-019-09539-6.

72. van Ham, T.J., Kokel, D., and Peterson, R.T. (2012). Apoptotic cells are cleared by directional migration and elmo1- dependent macrophage engulfment. Curr. Biol. *22*, 830–836. https://doi.org/10.1016/j.cub.2012.03.027.

73. Nakajima, Y.I., Kuranaga, E., Sugimura, K., Miyawaki, A., and Miura, M. (2011). Nonautonomous Apoptosis Is Triggered by Local Cell Cycle

Progression during Epithelial Replacement in Drosophila. Mol. Cell Biol. *31*, 2499–2512. https://doi.org/10.1128/Mcb.01046-10.

74. Teng, X., Qin, L., Le Borgne, R., and Toyama, Y. (2017). Remodeling of adhesion and modulation of mechanical tensile forces during apoptosis in Drosophila epithelium. Development *144*, 95–105. https://doi.org/10.1242/dev.139865.
75. Ohsawa, S., Vaughen, J., and Igaki, T. (2018). Cell Extrusion: A Stress-Responsive Force for Good or Evil in Epithelial Homeostasis. Dev. Cell *44*, 532. https://doi.org/10.1016/j.devcel.2018.02.007.
76. Levayer, R., Dupont, C., and Moreno, E. (2016). Tissue Crowding Induces Caspase-Dependent Competition for Space. Curr. Biol. *26*, 670–677. https://doi.org/10.1016/j.cub.2015.12.072.
77. Gurley, K.A., Rink, J.C., and Sánchez Alvarado, A. (2008). Beta-catenin defines head versus tail identity during planarian regeneration and homeostasis. Science *319*, 323–327. https://doi.org/10.1126/science.1150029.
78. Stirling, D.R., Swain-Bowden, M.J., Lucas, A.M., Carpenter, A.E., Cimini, B.A., and Goodman, A. (2021). CellProfiler 4: improvements in speed, utility and usability. BMC Bioinf. *22*, 433. https://doi.org/10.1186/s12859-021-04344-9.
79. Schindelin, J., Arganda-Carreras, I., Frise, E., Kaynig, V., Longair, M., Pietzsch, T., Preibisch, S., Rueden, C., Saalfeld, S., Schmid, B., et al. (2012). Fiji: an open-source platform for biological-image analysis. Nat. Methods *9*, 676–682. https://doi.org/10.1038/Nmeth.2019.
80. Berg, S., Kutra, D., Kroeger, T., et al. (2019). ilastik: interactive machine learning for (bio)image analysis. Nat Methods *16*, 1226–1232. https://doi.org/10.1038/s41592-019-0582-9.
81. Arzt M., Deschamps J., Schmied C., Pietzsch T., Schmidt D., Tomancak P., Haase R., Jug F. LABKIT: Labeling and Segmentation Toolkit for Big Image Data. Front. Comput. Sci. 2022;4:777728. https://doi.org/10.3389/fcomp.2022.777728.
82. King, R.S., and Newmark, P.A. (2013). In situ hybridization protocol for enhanced detection of gene expression in the planarian Schmidtea mediterranea. BMC Dev. Biol. *13*, 8. https://doi.org/10.1186/1471-213x-13-8.

STAR★METHODS

KEY RESOURCES TABLE

REAGENT or RESOURCE	SOURCE	IDENTIFIER
Antibodies		
Anti-Digoxigenin-POD, Fab fragments	Roche	Cat# 11207733910; RRID:AB_51450
Peroxidase-conjugated IgG Fraction Monoclonal Mouse-Anti Fluorescein (FITC)	Jackson Immuno Research Labs	Cat# 200032037; RRID:AB_2314402
Anti-Fluorescein-POD, Fab fragments	Roche	Cat# 11426346910 RRID:AB_840257
Chemicals, peptides, and recombinant proteins		
CellTracker™ Deep Red Dye	Invitrogen	Cat# C34565
CellTracker™ Red CMTPX Dye	Invitrogen	Cat# C34552
CellTrace™ CFSE Cell Proliferation Kit	Life Technologies	Cat# 6585084
CellTrace Far Red DDAO-SE	Invitrogen	Cat# C34553
Chloroquine Diphosphate Salt	Sigma-Aldrich	Cat# C6628
Ciprofloxacin	Sigma-Aldrich	Cat# 17850
DAPI	Thermo Scientific	Cat# 62247
DIG RNA labeling mix	Roche	Cat# 11277073910
NEBuilder® HiFi DNA Assembly Master Mix	New England BioLabs	Cat# E2621S
Halocarbon oil 700	Sigma-Aldrich	Cat# H8898
Linalool	Sigma-Aldrich	Cat# L2602
N-Acetyl-L-cysteine	Sigma-Aldrich	Cat# A7250
Paraformaldehyde 16% solution, EM grade	Electron Microscopy Sciences	Cat# 15710
Reddot1™ Far-Red Nuclear Stain, 200X in water	Biotium	Cat# 40060
SeaPlaque™ Agarose	Lonza	Cat# 50100
Experimental models: Organisms/strains		
Schmidtea mediterranea	A. Sánchez Alvarado	CIW4
Recombinant DNA		
pPR-T4P vector	Gurley et al.[77]	N/A
Software and algorithms		
Affinity Designer	Serif Ltd	v 1.10.5.1342; RRID:SCR_016952
CARE (csbdeep)	Weigert et al.[48]	v 0.7.2
CellProfiler	Stirling et al.[78]	v 4.2.5; RRID:SCR_007358
FIJI	Schindelin et al.[79]	v 2.14.0; RRID:SCR_002285
Ilastik	Berg et al. [80]	v 1.3.3post3; RRID:SCR_015246
Labkit	Arzt et al.[81]	v 0.3.10
IMARIS	Oxford Instruments	v 10.1; RRID:SCR_007370
Premosa	Blasse et al.[34]	initial release
Prism	GraphPad Software	v 10; RRID:SCR_002798
Stardist	Schmidt et al.[35]	v 0.5.0
Other		
CellRad Precision Irradiator	Precision X-RAY irradiation	N/A
DX845 PMP TPX Film 0.5mm thick 420mm coil W TPX®	GoodFellow	Cat# ME31-FM-000350
μ-Dish 35mm	ibidi	Cat# 81158

RESOURCES AVAILABILITY

Lead contact

Further information and requests for resources and reagents should be directed to and will be fulfilled by the lead contact, Jochen C. Rink (jochen.rink@mpinat.mpg.de).

Materials availability

This study did not generate new materials.

Data and code availability

- The Stardist models for the epidermal cell segmentation are available from the lead contact upon request.
- This paper does not report original code.
- Any additional information required to reanalyze the data reported in this work paper is available from the lead contact upon request.

EXPERIMENTAL MODEL AND STUDY PARTICIPANT DETAILS

All experiments were performed on the asexual strain of *Schmidtea Mediterranea* (CIW4). The animals were cultured in planarian water (1.6 mM NaCl, 1.0 mM $CaCl_2$, 1.0 mM $MgSO_4$, 0.1 mM $MgCl_2$, 0.1 mM KCl and 1.2 mM $NaHCO_3$ in Milli-Q water) containing 5 μg/mL Ciprofloxacin in plastic boxes at 20°C. The worms were fed with macerated calf liver once every two weeks. Animals were last fed 1 week or 2 weeks before the experiments depending on the designs of the experiments.

METHOD DETAILS

X-Ray irradiation

2 mm worms were selected and irradiated with X-ray at a dosage of 6000 rad using the CellRad Precision Irradiator. The worms were rinsed twice with planarian water containing 5 μg/mL ciprofloxacin immediately after irradiation exposure and planarian water was then refreshed daily.

Cloning and probe synthesis

The target genes, *dd_Smed_v6*: dd_75_0_1 and *dd_Smed_v6*: dd_115_0_1 , were amplified from *Schmidtea mediterranea* cDNA with gene-specific primer pairs (Table 1) and inserted into the pPR-T4P vectors using Gibson assembly. These constructs were used for *in situ* hybridization probe synthesis later. Linear DNA amplified by PCR from the gene-inserted plasmids were used as the templates for anti-sense probe synthesis. *In vitro* transcription for probe synthesis was performed by incubating 1 μg DNA template, 1X *in vitro* transcription buffer (25 mM $MgCl_2$, 40 mM Tris pH 8.0, 10 mM DTT, 2 mM spermidine), 1X DIG RNA labeling mix (Roche) or Fluorescein RNA labeling mix (Sigma-Aldrich), 1 U/μL RNAse inhibitor (Thermo Scientific), 0.0015 U/μL Inorganic Pyrophosphatase (Thermo Scientific) and 2 U/μL T7 polymerase (Thermo Scientific) together at 37°C overnight. The probe RNA was then precipitated by mixing the *in vitro* transcription mixture (20 μL) with 10 μL 7.5 mM ammonium acetate and 50 μL ice-cold 100% EtOH. After centrifugation, the RNA pellets were resuspended in deionized Formamide (AppliChem).

Whole-mount *in situ* hybridization

Whole-mount *in situ* hybridization was conducted as described previously in King & Newmark, 2013[82] with a few modifications: In brief, worms were euthanized in 5% NAC in PBS, fixed in 4% PFA in 50% PBS containing 0.15% Triton X-100. Worms were soaked in reduction solution (1% NP-40, 0.5% SDS, 50 mM DTT in 1XPBS in H_2O) at 37°C for 10 min and dehydrated in 100% MeOH. After rehydration in PBS containing 0.3% Triton X-100, worms were bleached in bleaching solution (1.2% H_2O_2, 5% formamide, 0.5XSSC in H_2O) on a light table for 1 h and treated with 2 μg/mL Protease K (NEB) in PBS containing 0.3% Triton X-100 for 10 min followed by post-fixation in 4% PFA for 10 min. The samples were soaked in Pre Hybe (50% Formamide, 5X SSC, 1X Denhardts, 100 μg/μL Heparin, 1% Tween 20, 1 mg/mL torula yeast RNA, 50 mM DTT) at 58°C for 2 h and were incubated in Hybe (50% Formamide, 5X SSC, 1X Denhardts, 100 μg/μL Heparin, 1% Tween 20, 0.25 mg/mL torula yeast RNA, 50 mM DTT, 0.05 g/mL dextran sulfate) with RNA probes at 58°C overnight. The next day, samples were washed with Wash Hybe (50% Formamide, 0.5% Tween 20, 5XSSC, 1 X Denhardts) twice; 1:1 Wash Hybe: 2XSSC (0.1% tween 20) twice; 2XSSC (0.1% tween 20) three times; 0.2XSSC (0.1% tween 20) three times at 58°C. Samples were soaked in blocking solution (5% sterile horse serum, 0.5% Roche western blocking reagent in TNTx) for 2 h at room temperature. Following blocking, samples were incubated with antibody (anti-DIG-POD, anti-FITC-POD or anti-Fluorescein-POD) in blocking solution (1:1000 from the antibody stocks) at 4°C overnight. For fluorophore development, samples were washed with TNTx (0.1 M Tris pH 7.5, 0.15 M NaCl, 0.3% Triton X-100 in H_2O) six times and proceed to tyramide amplification by incubating in TSA buffter (2M NaCl, 0.1M Boric acid in H_2O, pH8.5) containing 0.006% H_2O_2, 20 μg/mL 4-Iodophenylboronic acid and tyramide (Rhodamine or FAM) for 45 min at room temperature. For CFSE-labeled worms, CFSE signals were amplified by incubating in anti-FITC-POD antibodies (1:1000) in blocking solution and the fluorophore was developed by tyramide amplification (Rhodamine).

The peroxidase activity of the first antibody was quenched by incubation in 100 mM sodium azide in TNTx for at least 1 h at room temperature. The color reaction of the second antibody was developed like the first one. After color development, samples were soaked in Scale S4 (10% Glycerol, 15% DMSO, 40% Sorbitol, 4 M Urea, 2.5% DABCO, 0.1% Triton X-100 in H_2O) at 4°C overnight and mounted on slides the next day.

CFSE and DDAO labeling of the epidermis

Live-labeling of the epidermis with CFSE or DDAO was carried out by immersing the worms in planarian water containing 10 μM of CFSE or 1 μM of DDAO for 1.5 h at 20°C. Prior to fixation, the worms were euthanized in 5% N-Acetyl-L-cysteine in PBS for 3 min on a rotator and subsequently fixed in 100% MeOH at −20°C for 2 h. Following fixation, the samples were rehydrated sequentially with a series of MeOH concentrations in PBS: 75% MeOH, 50% MeOH and 25% MeOH. Nuclei were stained by immersing the worms in 5 μg/mL DAPI or 5 μg/mL Hoechst in PBS for 30 min at room temperature followed by three PBS rinses. Lastly, the samples were stored in 80% glycerol in PBS for at least 30 min at room temperate before being mounted between two of coverslips (24*60 mm, No. 1.5H and 22*22 mm, 1.5H; Schott) to allow for imaging from dorsal and ventral sides. For the cross-section samples, the specimens were mounted in 4% SeaPlaque agarose and cut into two pieces using a razor blade.

Sample preparation for live-imaging

Live-labeling of epidermal nuclei was carried out by immersing worms in planarian water containing containing 2x Reddot 1 and 1% DMSO in planarian water at 20°C overnight. For cytoplasmic live-labeling, worms were immersed in planarian water containing 1 μM CellTracker Deep Red Dye at 20°C for 1.5 h. To label the intestine, worms were fed with a fluorescent dye-containing liver paste mixture (20% liver paste, 0.3% SeaPlaque Agarose, 0.02 mM CellTracker Red CMTPX Dye in water; adopted from Forsthoefel et al., 2013[53]) one day prior to time-series imaging. Following labeling, the worms were anesthetized in 0.02% linalool at room temperature for 30 min. Mucus was removed by immersing worms in pH-neutralized 0.5% N-Acetyl-L-cysteine containing 0.02% linalool in distilled water for 10 s. Finally, worms were transferred to a μ-Dish 35 mm with a glass bottom and embedded in 1% SeaPlaque agarose containing 0.02% linalool. The agarose and sample were then covered with a PMP (Polymethylpentene) disc. The gap between the cover and glass bottom was sealed with halocarbon oil 700 to avoid drying of the embedding media.

Microscopy

Fixed samples were imaged using an Olympus IX83 microscope equipped with a Yokogawa CSUW1-T2S Spinning Disk system, which was fitted with a Hamamatsu Orca Flash4.0 V3 camera. Imaging was conducted with an Olympus UPLXAPO 10x air objective (NA = 0.4) or an Olympus UPLXAPO 20X air objective (NA = 0.8).

Live imaging was carried out on an Olympus IX83 microscope paired with a Yokogawa CSUW1-T2S Spinning Disk system and an Andor iXon Ultra 888 EMCCD camera. An Olympus UPLSAPO 60X Silicone objective (NA = 1.3) or an Olympus UPLSAPO 30X Silicone objective (NA = 1.05) were used. The samples were incubated in a thermostatic chamber at 15°C for the whole process of time-series imaging. Prior to capturing the time series images, animals were incubated in the chamber for 30 min. 100mW 640 nm and 100mW 561 nm excitation lasers were used for imaging with a laser power of 1% and an exposure time of 5 ms. The samples were scanned over a total z-depth of 30–60 μm with 1 or 2 μm section spacing. The z distance was set up 2–6 μm away from the specimens to the inside of the specimens. Z-stacks were recorded at 1-min intervals over a period of 3 h.

Visualization of time-series images

For the visualization of time-series images, the specific regions were selected and the signal-to-noise ratio was enhanced using the previously trained CARE models. To correct the drift of the sample over time, linear stack alignment with SWIFT in FIJI was used to align the images from single-color live-imaging recordings. Fast4DReg was used for the correction of two-color live-imaging. The depth of the z stack images was represented with different colors by the built-in color LUT (mpl-viridis) in FIJI.

Premosa surface extraction

Epidermal cells were extracted from 3D-image stacks of CFSE, DDAO and DAPI-labeled samples with Premosa software.[34] The DDAO signal, which labeled all epidermal cells, served as the surface reference for extracting the CFSE signal and nucleus signals of epidermal cells.

Stardist model training

To train Stardist models for cell segmentation, raw images and manually annotated images served as the input training pairs for training. The raw images consisted of the Premosa-processed CFSE images. For the ventral epidermis, images from non-irradiated and irradiated worms were used: Images were normalized to 0.3rd percentile pixel saturation and 256*256 pixel crops were randomly selected. For training images obtained from the dorsal epidermis, images were normalized to the 1st percentile pixel saturation and 256*256 pixel crops were randomly selected. The annotated images were generated by manually annotating individual epidermal cells in the raw images with the Fiji Plugin Labkit.[81] Additionally, each raw image and annotated image were additionally rotated by 90, 180, 270° and flipped. Therefore, 8 different raw and annotated images were generated from one original image by the rotation and flipping. For the training of the Stardist models, a total of 199*8 training pairs were used for training the ventral epidermis model,

Please cite this article in press as: Lee et al., Epidermal turnover in the planarian *Schmidtea mediterranea* involves basal cell extrusion and intestinal digestion, Cell Reports (2024), https://doi.org/10.1016/j.celrep.2024.114305

and 66*8 pairs were used for training the dorsal epidermis model. The detailed parameters for the training of the Stardist models are listed Table S1.

Stardist model verification

For Stardist model verification, 256*256 pixel crops were selected randomly in DDAO, CFSE and DAPI labeled images. Prior to cropping, the 1st or 3rd percentile of pixels were normalized to saturation in CFSE or DDAO-labeled images respectively. The detailed parameters for the Stardist model prediction are listed in Table S2. For the ventral epidermis, a 200 pixel size cut-off was set to eliminate undersegmented objects. The results from the model prediction were compared to the results from the ground truth (manual counting). The accuracy of the Stardist models was quantified using the following equation:

$$accuracy = 1 - \left| \frac{n_{prediction} - n_{ground\ truth}}{n_{ground\ truth}} \right|$$ where n represents the number of counted objects in the respective condition. For the turnover rate quantification, the same parameters as employed in the model verification were applied to the selected area.

CARE model training

To enhance the signal-to-noise ratio of time-series images, CARE models were trained using z stack images captured consecutively with short exposure time (5 ms) and long exposure time (100 ms). Two to five such image pairs were recorded prior to the time-lapse recording and used for training. Importantly, for each time course, a CARE model was specifically trained assuring the highest denoising accuracy for each sample. The parameters for training CARE models are listed in Table S3.

Drug treatment

For chloroquine treatments, 3 mm long worms were immersed in 5 μM chloroquine in planarian water containing 5 μg/mL Ciprofloxacin for 4 days and the epidermis was labeled with CFSE for 1 h on the fifth day of chloroquine treatment. The worms were then fixed 4 days after the CFSE labeling. Throughout the CFSE chase, worms were kept in planarian water with 5 μM chloroquine. As the control group, worms were cultured in plain planarian water. To visualize the intestine, worms were fed with fluorescent dye-containing liver paste (20% liver paste, 0.3% SeaPlaque Agarose, 0.02 mM CellTracker Deep Red Dye in water).

Image analysis and statistical analysis

Quantifications of intestinal volume, $CFSE^+$ object volume and $CFSE^+$ object numbers were carried out in the dorsal tips of intestinal branches in the head area. Greyscale images were transformed to binary masks with the threshold function in FIJI. The Huang model was used for thresholding. Objects that were smaller than 10 voxels were excluded from the analysis. To quantify the ratio of the $CFSE^+$ volume to total volume of the selected area, the mesenchymal area between the intestine and epidermis in the anterior region was selected. The volume of the 3D masks was quantified with standard CellProfiler pipelines.

For tracking and quantifying epidermal nuclei intensity and depth, cropped, CARE-restored and drift corrected z stack time series were processed with IMARIS software for tracking individual nuclei over time. In brief, objects were detected in 3D by intensity and size thresholding. The IMARIS-implemented object tracking function was used to track nuclei over time and to analyze their relative position and intensity throughout the time course. The depth or maximum intensity of each nucleus over time was normalized to the average depth or intensity of the first 10 min of each nucleus' recorded track.

To measure planarian sizes, animals were recorded with a Canon EOS 6D MarkII digital camera equipped with a SIGMA 150 mm F2,8 APO Makro EX DG OS HSM lens. A specifically trained ilastik software pixel classifier was used to segment the image. The area of each mask was quantified using Cellprofiler software.

Statistical details, including the representation of centers and error bars in graphs, are described in the figure legends. n refers to the number of animals or images analyzed as specified in the figure legends. Significance was determined by the Mann-Whitney-U test or t test with the p-value <0.05. The statistical analyses were conducted using Graphpad Prism software.